Article

Water Chemistry Impact on Activated Corrosion Products Assessment in Tokamak Reactors

Martina Molinari [1*], Matteo D'Onorio [1], Giovanni Mariano [2], Nicholas Terranova [2] and Gianfranco Caruso [1*]

[1] Sapienza University of Rome, Department of Astronautical, Electrical and Energy Engineering (DIAEE) – Nuclear Section, Corso Vittorio Emanuele II 244, 00186 Roma, Italy;
[2] ENEA Fusion and Technology for Nuclear Safety and Security Department, CR Frascati, Via Enrico Fermi 45, 00044 Frascati, Italy;
* Correspondence: martina.molinari@uniroma1.it; gianfranco.caruso@uniroma1.it

Abstract: Activated Corrosion Products (ACPs) formation and deposition pose a critical safety issue for nuclear fusion reactors. The working fluid transports the ACPs towards regions accessible to worker personnel. Predicting ACPs formation deposition and transport is fundamental for source term identification, reduction of radiation exposure assessment, maintenance plan definition, design optimization, and waste management. The code OSCAR-Fusion has been developed by the CEA (France) to evaluate the ACPs generation and transport in closed water-cooled loops for fusion application. This work aims at assessing the impact of water chemistry on the transport, precipitation, and deposition of corrosion products for the EU-DEMO divertor Plasma Facing Unit Primary Heat Transfer System. Sensitivity analyses and uncertainty quantification are needed due to the multi-physics phenomena involved in ACPs formation and transport. The OSCAR-Fusion/RAVEN code coupling developed by the Sapienza University of Rome and ENEA has been used. This work presents the perturbation results of different parameters chosen for a closed water-cooled loop considering a continuous scenario of 1888 days. The aim of this work is to assess the variation of build-up of ACPs, perturbing the alkalizing agent concentration into the coolant and the corrosion and release rates of different materials.

Keywords: Activated Corrosion Products; Water Chemistry; OSCAR; RAVEN; Nuclear Safety

1. Introduction

The ACPs evaluation plays a fundamental role in the safety assessment of fusion reactors [1]. When considering the radioactive contamination of a cooling system of a nuclear plant, the ACPs study is helpful for the optimization of plant operation and, at the same time, the reduction of occupational radiation exposure when the source term is considered. Moreover, the source term, including ACP, can be mobilized during accident scenarios [2,3].

The ACPs generation and transport processes depend on several physical phenomena involving neutronics, thermal-hydraulic, chemical, and geometry aspects. There are several computational tools for the evaluation of ACPs generation and transport. One of these is OSCAR-Fusion [4], developed by the CEA to study the contamination of cooling circuits in the PHTS of a tokamak reactor.

In each region of the loop, there are two different oxide layers above the base metal: the inner one is adherent to the base metal and is a chromite layer, an oxide mineral composed of chromium oxide with iron oxide (Cr_2FeO_4). The second layer, located above the chromite layer, is a ferrite porous medium layer, an oxide mineral rich in ferric oxide

Preprints (www.preprints.org) | NOT PEER-REVIEWED | Posted: 12 April 2023 doi:10.20944/preprints202304.0275.v1

(Fe_2O_3). In the coolant, there are also particles and ions which are produced by erosion and dissolution mechanism. These particles and ions transported throughout the loop may precipitate or dissolve depending on the equilibrium concentration of elements or particles [5].

In a closed loop of a tokamak reactor, because of coolant transport, the corrosion products are carried from the Out-Flux (OF) region to the In-Flux (IF) region and vice versa. The corrosion products produced in the OF region will be activated in the IF region, and the ones produced in the IF region, activated under direct neutron flux, will contaminate the structural material in the OF region.

OSCAR-Fusion allows the study of generation, transport, and activation phenomena to assess the mass associated with an isotope in a given medium at a specific time for each region of the loop. The mass variation is correlated to the various physical mechanisms considered in OSCAR-Fusion and the chemical characteristic of both materials and coolant.

Radiolysis is caused by the presence of radiation fields, which result in high oxidizing products [6]. The minimization of the corrosion product built up into a loop can be achieved by optimizing the coolant water chemistry, which can control corrosion phenomena through alkalizing agents and elements able to suppress the oxidizing environment established because of radiolysis.

The alkalizing agents considered for the reducing environment of a PWR, as described in [7], are lithium hydroxide (LiOH), potassium hydroxide (KOH), and ammonia (NH_3) with variable concentrations, depending on boric acid concentration (H_3BO_3) used for reactivity control. In a nuclear fusion reactor, the presence of H_3BO_3 is not foreseen, but radiolysis is expected because of the high neutron flux.

For this reason, an alkalizing agent is expected [8] for pH control and oxidizing environment suppression.

Different experimental analysis has been performed [9] to optimize the water chemistry of tokamak reactors.

The aim of this paper is to study the impact of water chemistry on ACPs generation and transport for a closed loop by perturbing specific parameters that characterize the coolant's chemical composition. This analysis can be done thanks to a code interface OSCAR-Fusion/RAVEN described in [10] and a Python-based post-processing script.

2. OSCAR-Fusion V1.3

OSCAR-Fusion is a one-dimensional code that can use physical models implemented for corrosion products to study the mass exchange between the media and the control volumes modelled. Like the previous versions of the code as PACTITER, or the ones used in fission (e.g., OSCAR and PACTOLE), described in [4,11,12], the evaluation of ACPs is based on the masses balance equation. The variation of a mass M, of the isotope i in a given medium j at time t, for a control volume, comes from the mass balances conservation equation [5]:

$$\frac{\partial M_i^j}{\partial t} = \sum Source - \sum Sink + \dot{m}_\iota - \dot{m}_o \quad (1)$$

Preprints (www.preprints.org) | NOT PEER-REVIEWED | Posted: 12 April 2023 doi:10.20944/preprints202304.0275.v1

where $\dot{m}_i$ and $\dot{m}_o$ are the control volumes inlet and outlet flow rates.

As described in [5], the media considered are the base metal, the inner oxide layer, the deposit/outer oxide layer, ions, particles, filters, and resins.

Each control volume can describe a closed-loop region, considering given input parameters as thermal-hydraulic, neutronic, power distribution, and water chemistry.

The thermal-hydraulic data of the OSCAR-Fusion V1.3 are evaluated by the same formulation of the CATHARE code, which is optionally used to evaluate the fluid velocity and the density, both temperature dependent. The PHREEQCEA module evaluates the chemical data.

In OSCAR-Fusion V1.3, the water chemistry characteristics can be evaluated by setting lithium, boron, hydrogen, and oxygen concentration for each period. In OSCAR-Fusion, the lithium concentration corresponds to a lithium hydroxide (LiOH) concentration in water, the boron concentration corresponds to a boric acid (H_3BO_3) concentration in water, and hydrogen and oxygen concentration correspond respectively to molecular hydrogen (H_2) and molecular oxygen (O_2) in water. It must be highlighted that OSCAR-Fusion V1.3 does not foresee physical models for radiolysis, which is caused by the radiation field.

In OSCAR-Fusion V1.3, corrosion and release rates can be evaluated by setting specific parameters, such as the standardized coefficients for the Short Term Corrosion Rate (STCR) and the Long Term Corrosion Rate (LTCR), the temperature of the coolant and the water chemistry characteristics.

In the OSCAR-Fusion code, the default correlations for corrosion rate and release rate are the Moorea laws. The Moorea laws are empirical laws and, for both corrosion rate and release rate, depending on four factors: the standardized coefficient STCR and LTCR, a function of the temperature of the fluid, a function related to pH of the fluid, and an attenuation factor which in turn depends on ion concentration of a metal species with respect to its equilibrium concentration.

3. EU-DEMO Divertor Plasma Facing Unit

The EU-DEMO divertor component is located in the bottom region of the torus. The divertor role is to reduce the heat flux on the first wall and the helium ashes from the plasma's outer layer, avoiding its build-up and dilution of the plasma ion density and preventing the impurities from entering the plasma core. The DEMO divertor system, as described in [13], is composed of two independent systems, as shown in Figure 1a, the DIVertor CASsette (DIV-CAS) and the DIVertor Plasma Face Unit (DIV-PFU). Both systems are composed of two independent loops, each of them serving 8 of 16 sectors, according to the 2019 design of the Divertor PHTS. A single system of the loop comprises 24 divertor cassettes, three for each sector of the torus.

Preprints (www.preprints.org) | NOT PEER-REVIEWED | Posted: 12 April 2023 doi:10.20944/preprints202304.0275.v1

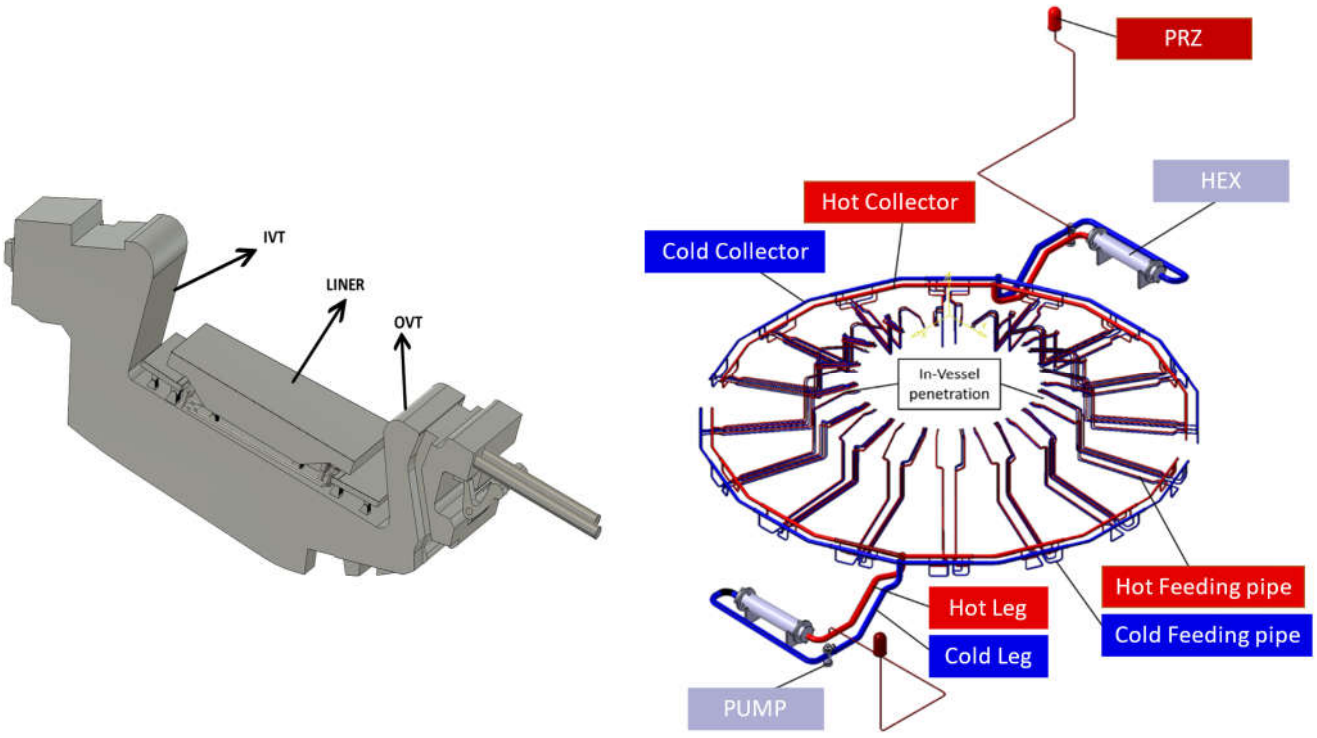

(**a**) (**b**)

Figure 1: (**a**) Divertor assembly; (**b**) Divertor PFU PHTS

The EU-DEMO divertor system PHTS components are shown in Figure 1b. Each PHTS loop consists of: one Heat EXchanger (HEX), one Main Coolant Pump (MCP), one PRessuriZer (PRZ), 8 distributors (DIS), 8 collectors (COL), 24 Hot Feeding Pipe (HFP), 24 Cold Feeding Pipes (CFP), one Hot Leg (HL), one Cold Leg (CL) and one Cross Over pipe (COV).

Each cooling loop of the divertor PFU PHTS is operated at a pressure of 3.8 MPa with a mass flow rate of 5319.3 kg/s 13 distributed over the 24 divertor cassette. The cooling water is distributed at 130 °C and is collected at 136 °C.

The divertor system PHTS also presents the Chemical Volume Control System (CVCS, named as BY in Figure 2), with mechanical filters and ion exchange resins, to maintain the coolant purity and chemical composition.

4. OSCAR-Fusion model of EU-DEMO Divertor PFU

The OSCAR-Fusion model of the divertor PFU PHTS is shown in Figure 2. The model is a simplified closed loop subdivided into 53 regions. Each region has assigned conditions of temperature, pressure, wetted surface, hydraulic diameter, and coolant velocity.

Preprints (www.preprints.org) | NOT PEER-REVIEWED | Posted: 12 April 2023 doi:10.20944/preprints202304.0275.v1

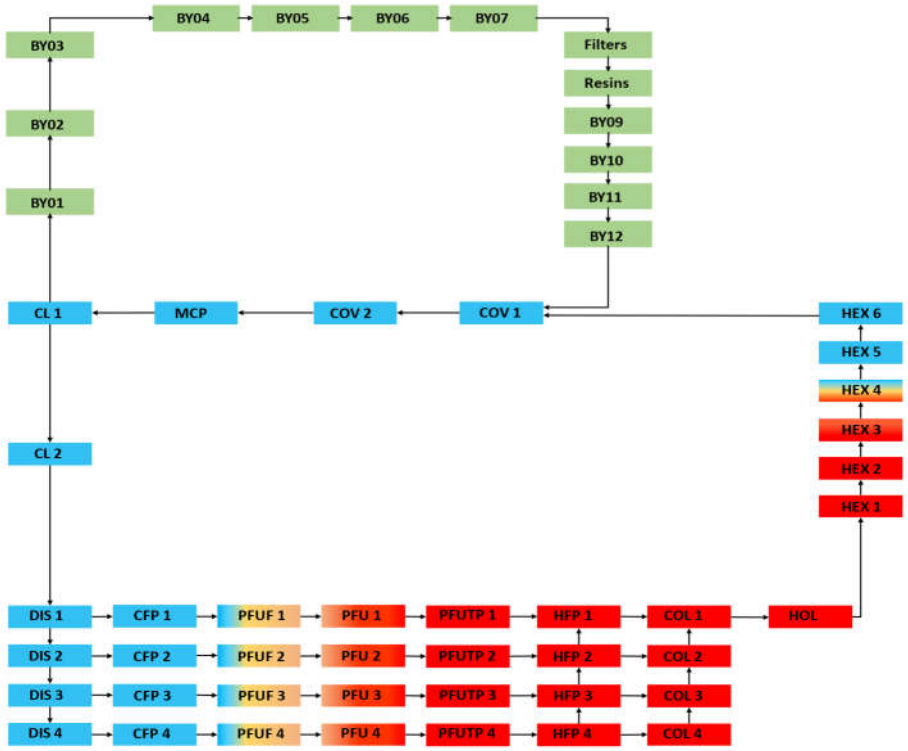

Figure 2: EU-DEMO divertor PFU PHTS model

As described in [14], since the CVCS design is not confirmed, some assumptions have been made during the modelling phase. The cooling loops are collapsed in half of a single cooling loop using equivalent thermal-hydraulic data. The filters and resin efficiency have been set to 99 %.

In the OSCAR-Fusion model of the divertor PFU PHTS, four different materials are considered as base metals: Inconel 660, stainless steel SS 316 LN, Metal Cu, and the CuCrZr alloy. For each material, the input chemical parameters are the base metal, the inner/outer oxide layers, and the normalized corrosion coefficients for the evaluation of the corrosion rate and release rate. The default normalized coefficients are shown in Table 1, where it can be seen that the coefficients are defined before 2 months, which is the STCR, and after 12 months, which is the LTCR. In the interval 2 - 12 months, coefficients are correlated between SCTR and LCTR values.

Table 1. Normalized coefficients for corrosion rate and release rate

Time [months]	Stainless Steel [g/s/m²]	Copper based alloy [g/s/m²]
t ≤ 2	1.6E-06	1.33E-06
t >12	4.6E-07	1.33E-06

The temperature and pressure variations inside the loop are imposed as input parameters. The temperature trend in the loop lies in a range of 130°C – 136°C. The pressure drop has been evaluated as 1.960 MPa, as described in 13. The water volume is

Preprints (www.preprints.org) | NOT PEER-REVIEWED | Posted: 12 April 2023 doi:10.20944/preprints202304.0275.v1

about 114 m^3, and its composition is reported in Table 2. The DEMO water chemistry optimization is preliminarily evaluated and has a pH of around 7 at 300°C [15]. The operational scenario adopted for the simulation is a lumped continuous scenario of 1888 days.

Table 2. Divertor PFU water chemistry parameter

Chemical parameter	Concentration
Lithium	0.275 ppm
Boron	0.01[1] ppm
Hydrogen	25 ml/kg_w
Oxygen	0 ppm

[1] Minimum value allowed in OSCAR-Fusion V1.3

Using the parameters shown in Table 2 as input, the pH trend in the loop, at the initial time of the considered scenario, assumes the values depicted in Figure 3a and Figure 3b. The pH values range in Figure 3a is kept close to neutrality, because the pH target is in range of 7.0 at the operating temperature of the loop.

A difference from neutrality is therefore preferable to a slightly alkaline environment because an acid pH can be reached during operating conditions due to temperature variations and radiolysis reactions.

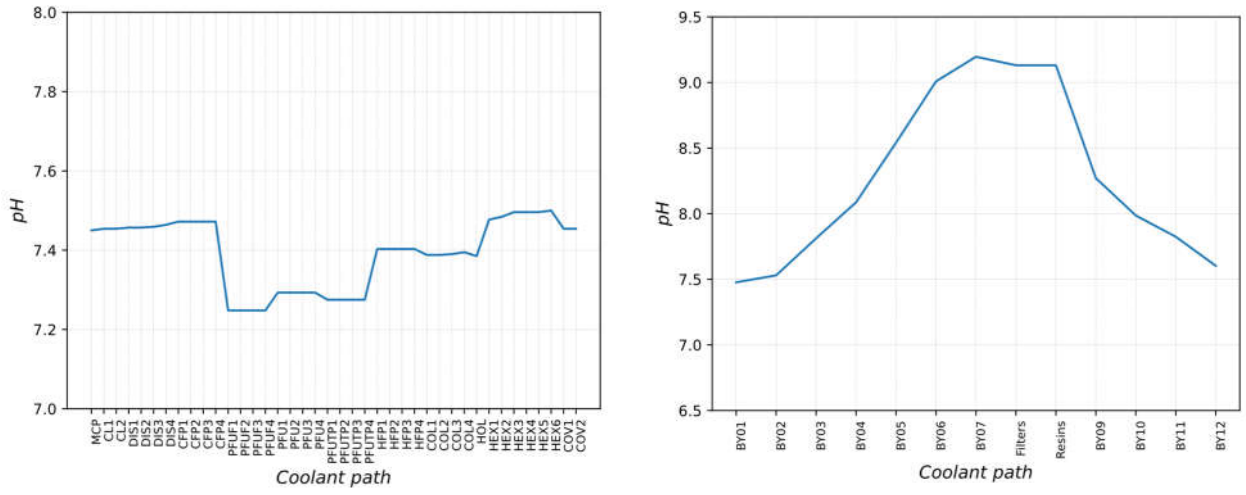

(**a**) (**b**)

Figure 3. pH trend of the reference case (**a**) in the loop; (**b**) bypass line

5. RAVEN/OSCAR-Fusion analyses

A statistical study with RAVEN/OSCAR-Fusion has been performed to assess the impact of water chemistry on ACPs generation and transport.

RAVEN is a multi-purpose, probabilistic, and uncertainty framework developed at the Idaho National Laboratory (INL), which can be coupled with any system code [16,17]. The RAVEN/OSCAR-Fusion interface has already been tested for a preliminary study, as reported in [10].

Preprints (www.preprints.org) | NOT PEER-REVIEWED | Posted: 12 April 2023 doi:10.20944/preprints202304.0275.v1

To perform the sensitivity analysis, the parameters that have to be studied and perturbed must be identified. This study's parameters are the lithium concentration and hydrogen concentration in the cooling water. The Figure of Merit (FOM) chosen to evaluate the perturbation's effect is the Mn-54 in the deposit/outer oxide layer medium. The Mn-54 reactions, decay mode, and energy of the γ emitted are summarised in Table 3.

For both case studies, 100 runs were performed. The total number of runs has been evaluated using Wilk's formula, as described in [18,19]. Pearson's and Spearman's coefficients have been used to quantify the correlation between the variables 2021.

Table 3. Mn-54 reactions and decay characteristics

Reactions	Father	Decay mode	Daughter	Energy [keV]	$T_{\frac{1}{2}}$ [d]
Mn-53(n, γ) Mn-54 Mn-55(n, 2n) Mn-54 Fe-54(n, p) Mn-54 Fe-54(n, np)Mn-53(n, γ) Mn-54	Mn-54	Electronic capture	Cr-54	834.855	312.19

6. Results for Case Study 1: Lithium concentration

The lithium concentration has been perturbed starting from the divertor system's water chemistry parameters summarized in Table 2.

The lithium concentration represents the only alkalizing agent which can be simulated in OSCAR-Fusion V1.3. The perturbation of LiOH concentration in water means a variation in pH and, therefore, the increase or reduction of the corrosion rate. The perturbation of lithium concentration is reported in Table 4.

Table 4. Case Study 1 - sampling

Lithium concentration (Uniform distribution) [ppm]	
Lower Bound (LB)	Upper Bound (UB)
0.0	1.5[2]

[2] Maximum value allowed in OSCAR-Fusion V1.3

The 100 runs completed by the code have been statistically analyzed, showing that the lithium concentration perturbation has led to a range of values depicted in Figure 4a and Figure 4b. It is possible to notice a trend in which the pH increases when the concentration of LiOH increases.

Preprints (www.preprints.org) | NOT PEER-REVIEWED | Posted: 12 April 2023 doi:10.20944/preprints202304.0275.v1

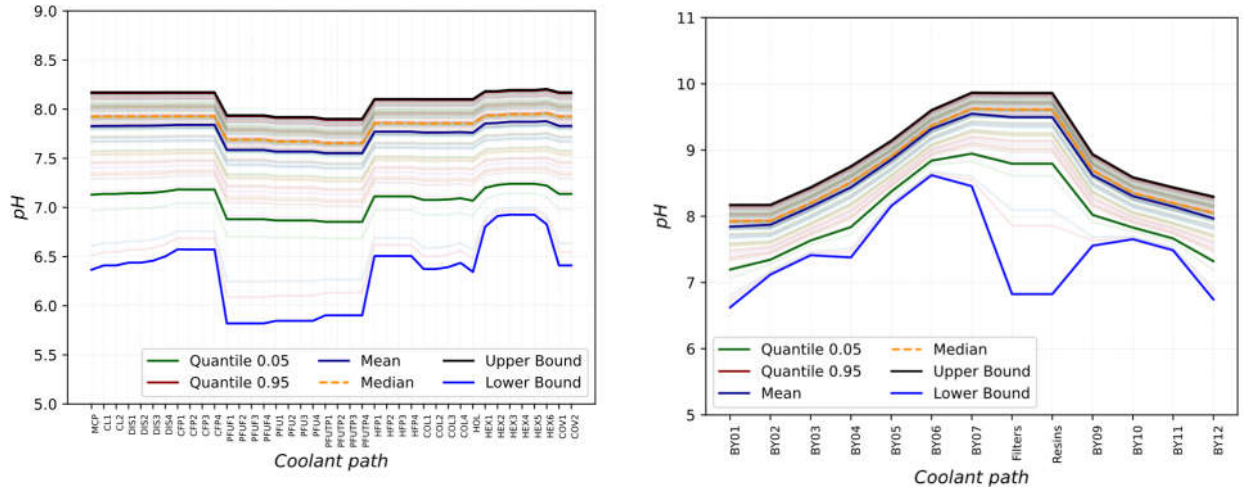

(**a**) (**b**)

Figure 4. pH trend after Li concentration perturbation (**a**) in the loop; (**b**) bypass line

Because Mn-54 can also be obtained from Fe-54, both Mn and Fe corrosion rates must be considered. During the entire simulation, there is a variation in the corrosion rate of both Mn and Fe in the deposit/outer oxide layer medium caused by pH variation. By varying the corrosion rate, the deposit/outer oxide layer formation mechanism increases. Figure 5a shows the main statistical parameters evaluated for the FOM.

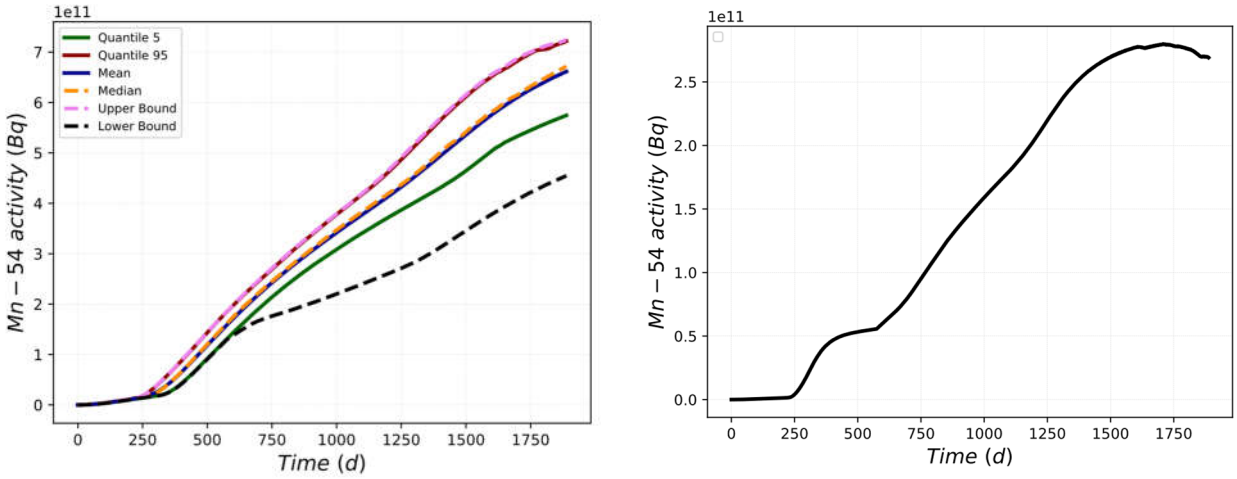

(**a**) (**b**)

Figure 5. (**a**) Mn-54 activity in the deposit/outer oxide layer; (**b**) Mn-54 activity difference between UB and LB

As can be seen in Figure 5b the difference between the UB trend and the LB trend is time-dependent. Figure 5b shows a maximum difference of 2.79E+11 Bq and a difference at the end of the scenario of 2.69E+11 Bq.

The analyzed data increasingly deviate from the trend of the mean value. Figure 6a shows the mean value trend, while Figure 6b depicts the standard deviation trend of the Mn-54 activity into the loop. The standard deviation trend is also predictable from Figure

Preprints (www.preprints.org) | NOT PEER-REVIEWED | Posted: 12 April 2023 doi:10.20944/preprints202304.0275.v1

5a. The data's variability increases at about 600 days and tends to reduce at about 1500 days. This reduction is also confirmed by the variation in the slope of the first derivative in the same moments as in Figure 5b.

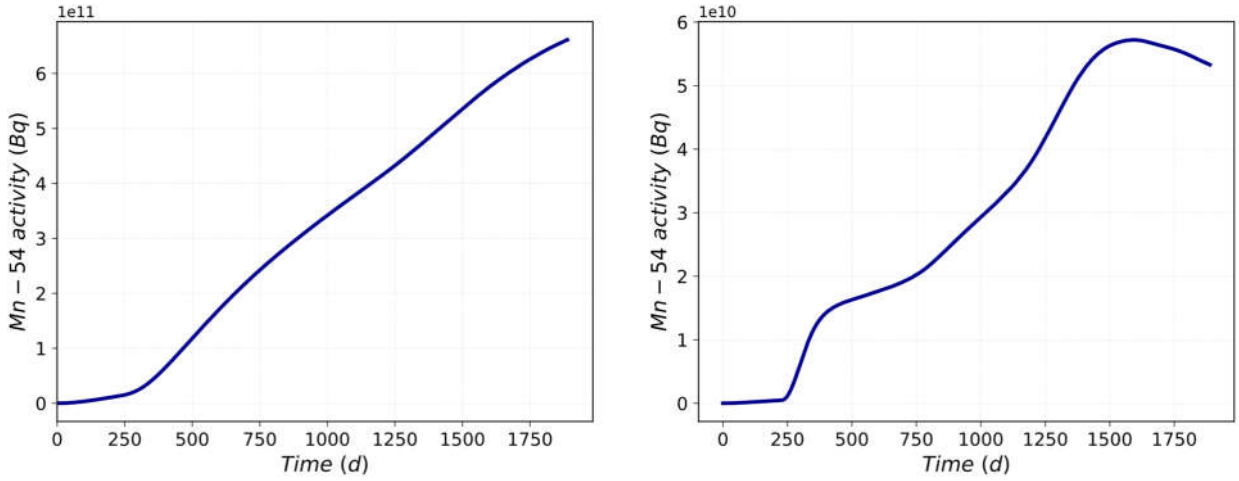

(**a**) (**b**)

Figure 6. Mn-54 activity (**a**) mean value trend; (**b**) standard deviation trend

In Figure 7, the Probability Density Function (PDF) evaluated at the end of the scenario is shown. A platykurtic and non-symmetric distribution, centered in 6.61E+11 Bq, is obtained. The PDF characteristics are confirmed by the Kurtosis and Skewness values reported in Table 5.

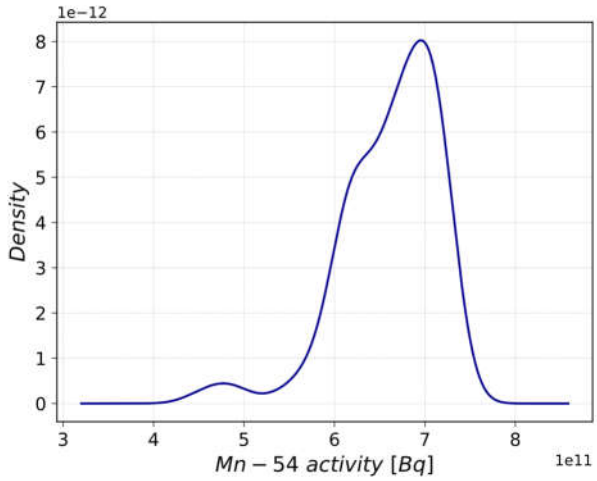

Figure 7. PDF

Table 5. PDF description factors

Kurtosis	-1.38	k<0: the PDF is platykurtic
Skewness	0.54	s>0: data are skewed to the righ

Preprints (www.preprints.org) | NOT PEER-REVIEWED | Posted: 12 April 2023 doi:10.20944/preprints202304.0275.v1

Figure 8a and Figure 8b highlight that perturbing the LiOH concentration, there is a variation in the Mn54 activity in the deposit medium. After 3 days from the beginning of the scenario, the correlation between the perturbed parameter and the FOM is at the highest value, as shown in Figure 9a and Figure 9b by Pearson's and Spearman's correlation coefficients. Pearson's correlation is a measure of linear correlation between two sets of data [21], instead the Spearman's correlation is the measure of monotonic relation between the ranked values of two sets of data [20]. This means that the correlation between the LiOH concentration perturbation and Mn – 54 activity in the deposit/outer oxide layer is neither linear nor monotonic, and there is a weak correlation between the LiOH concentration and the FOM.

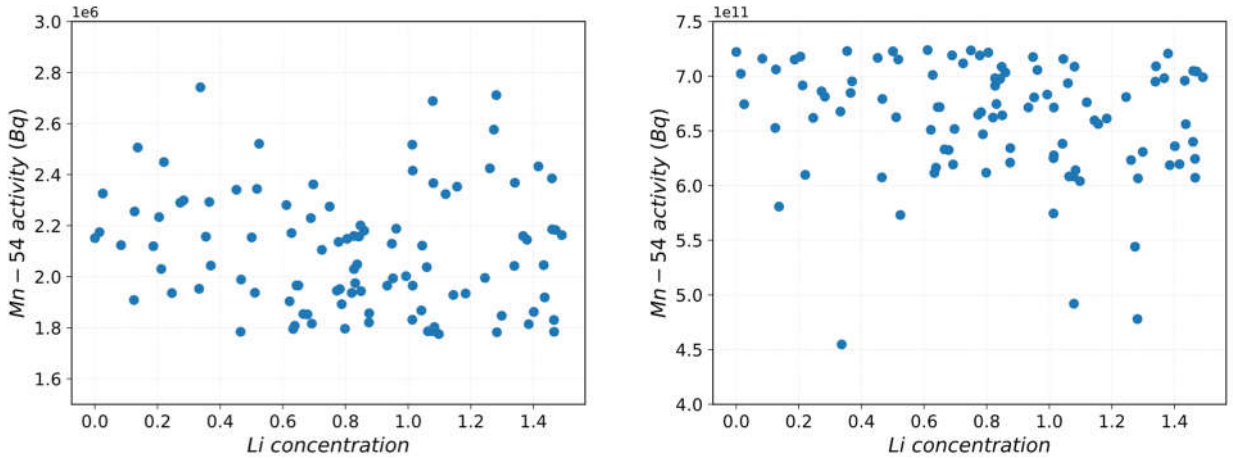

(**a**) (**b**)

Figure 8. Mn-54 activity vs. Li concentration (**a**) after 3 days; (**b**) after 1888 days

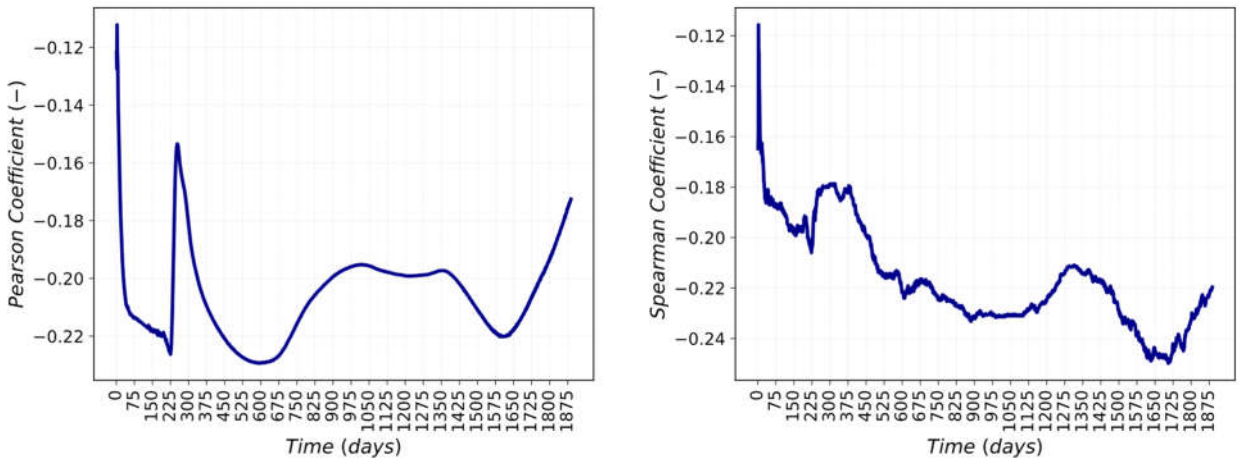

(**a**) (**b**)

Figure 9. Correlations between Mn-54 activity in deposit and Li concentration (**a**) Pearson; (**b**) Spearman

Preprints (www.preprints.org) | NOT PEER-REVIEWED | Posted: 12 April 2023 doi:10.20944/preprints202304.0275.v1

7. Results for Case Study 2: Corrosion Rates

When editing the laws of corrosion and release models, the OSCAR-Fusion code requires several parameters, some of which are the standardized coefficient for corrosion rates for copper-based alloy and stainless steel. The default parameters are shown Table 2.

In order to evaluate the CPs formation and activation, the standardized coefficients for corrosion rates has been taken into account. The perturbation of the standardized coefficient for corrosion rates is reported in Table 6. For Cu-based alloy, the UB and LB have been chosen considering the oxidizing condition described in [22] at 130°C and a fluid velocity of 13 $^{m}/_{s}$. The UB and LB values have been selected in order to have a not negligible perturbation on the corrosion rate and release rate of the materials considered into the loop.

Table 6. Case Study 2 - sampling

Standardised coefficients for corrosion rates (Uniform distribution) [g/m²/s]		
Coefficient	**UB**	**LB**
Copper based alloy	1.22E-05	7.67E-06
Stainless Steel STCR	5E-06	5E-07
Stainless Steel LTCR	1E-06	1E-07

The 100 runs completed by the code have been statistically analyzed and, as in the previous case, Mn and Fe corrosion rates have been considered. During the entire simulation, there is a variation in the corrosion rate in the deposit/outer oxide layer caused by the induced perturbation. By varying the corrosion rate, the deposit/outer oxide layer formation mechanism increases.

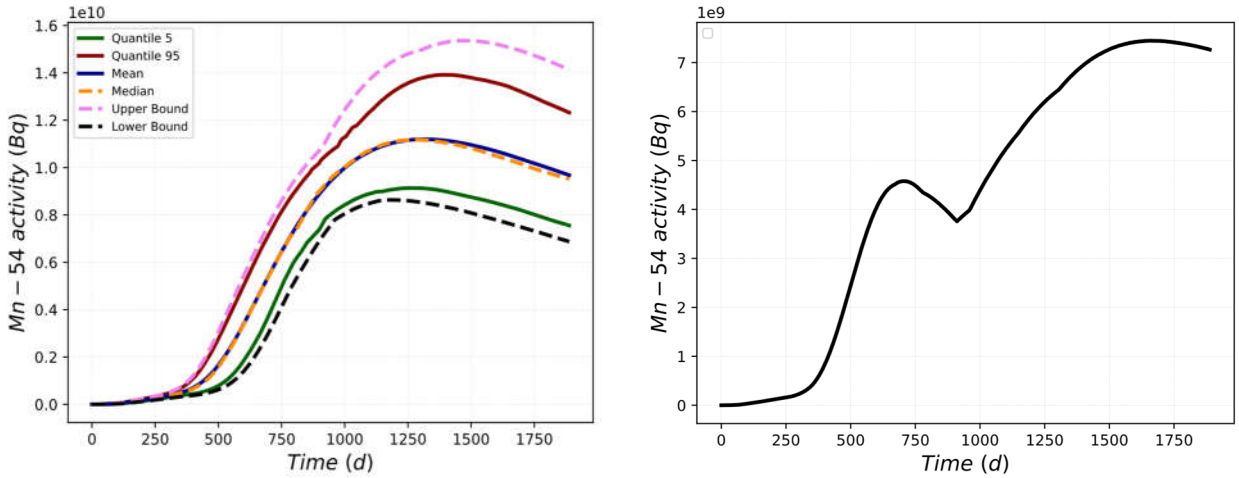

(**a**) (**b**)

Figure 10. Mn-54 activity (**a**) statistical parameters; (**b**) difference between UB and LB

Preprints (www.preprints.org) | NOT PEER-REVIEWED | Posted: 12 April 2023 doi:10.20944/preprints202304.0275.v1

Figure 10a shows the main statistical parameters evaluated for the selected FOM, the Mn-54 activity in the deposit/outer oxide layer, while Figure 10b shows the difference in the activity of UB and LB. A maximum difference of 7.45E+09 Bq and of 7.26E+09 Bq at the end of the considered scenario have been obtained.

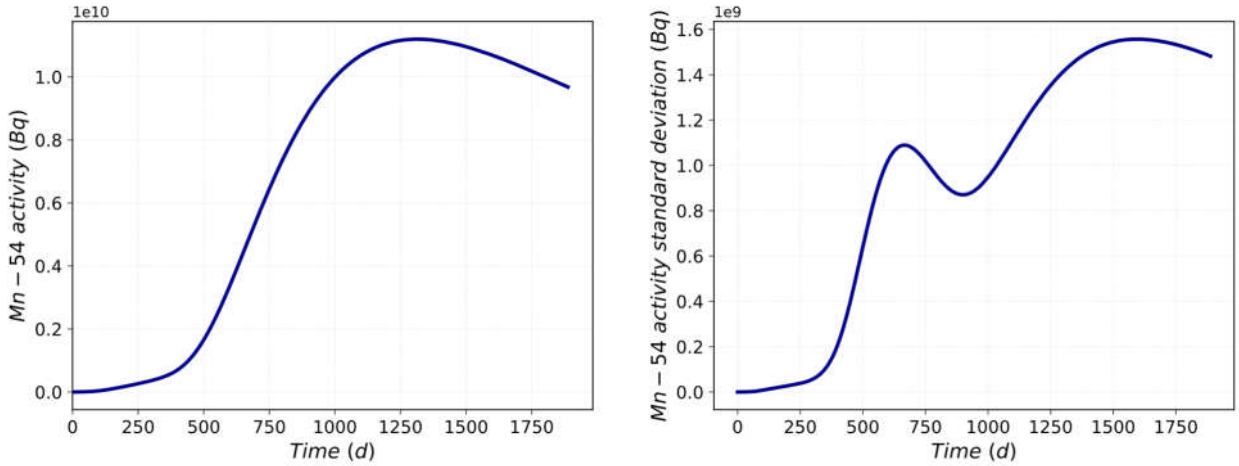

(**a**) (**b**)

Figure 11. Mn-54 activity trend (**a**) mean value; (**b**) standard deviation

In Figure 11a is shown the mean value trend, while Figure 11b depicts the standard deviation trend of the Mn-54 activity into the loop. It can be seen that the analyzed data deviation increases with time. The standard deviation trend is predictable, taking into account the statistical parameters. In Figure 10a, at about 400 days, there is an increase in the variability of the data up to the first point of maximum at about 700 days. After 700 days, there is a decrease until 900 days. After that, the standard deviation increases again until the second maximum point is reached, at about 1550 days. After 1550 days the variability of the data tends to reduce.

In Figure 12 the PDF evaluated at the end of the scenario is reported, showing a platykurtic and quasi-symmetric distribution, centered in 9.67E+09, which is the mean value. The PDF characteristics are confirmed by the Kurtosis and Skewness values in Table 7.

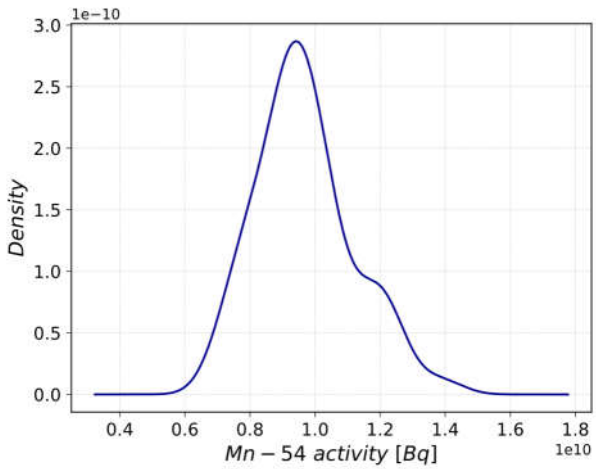

Figure 12. PDF

Preprints (www.preprints.org) | NOT PEER-REVIEWED | Posted: 12 April 2023 doi:10.20944/preprints202304.0275.v1

Table 7. PDF description factors

Kurtosis	-1.441	k<0: the PDF is platykurtic
Skewness	0.02	s>0: data are skewed to the righ

Figure 13, Figure 14a and Figure 14b highlight that perturbing the standardised coefficients for corrosion rate, there is a variation in the Mn-54 activity in the deposit medium.

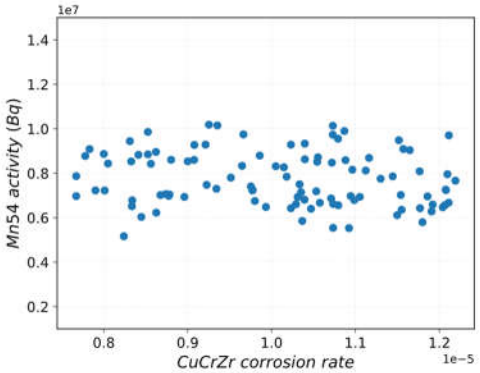

Figure 13. Mn-54 activity vs. CuCrZr corrosion rate sampling

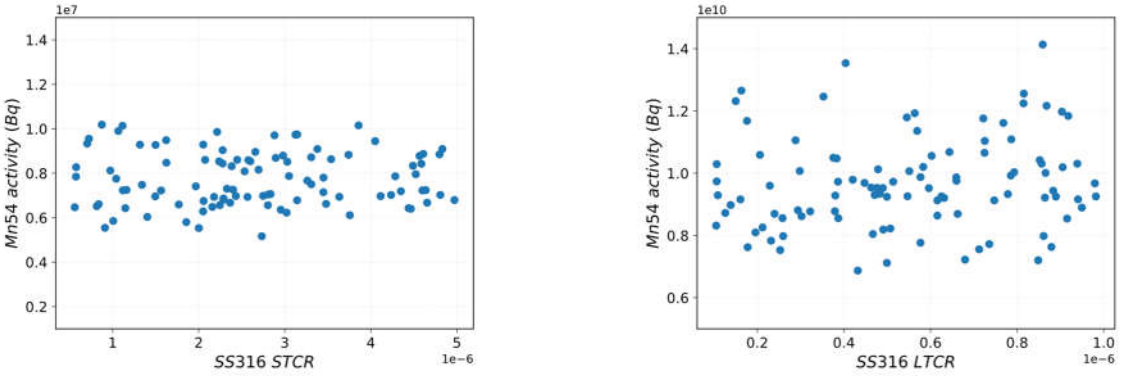

(**a**) (**b**)

Figure 14. Mn-54 activity vs. SS316 sampling (a) STCR; (b) LTCR

Pearson's and Spearman's partial correlations coefficients are shown in Figure 15, Figure 16a and Figure 16b. The correlation between the normalized coefficients of Cu-based alloy and Mn – 54 activity in the deposit/outer oxide layer is linear and monotonic from the beginning of the simulation until 800 days, and from 1000 days until the end of the scenario.

The correlation between the STCR and the Mn-54 activity in deposit/outer oxide layer is strong for the entire scenario considered, therefore it can be concluded that the correlation is both linear and monotonic.

The correlation between the LTCR and the Mn-54 activity in the deposit/outer oxide layer is linear and monotonic from about 900 days until the end of the scenario considered.

Preprints (www.preprints.org) | NOT PEER-REVIEWED | Posted: 12 April 2023 doi:10.20944/preprints202304.0275.v1

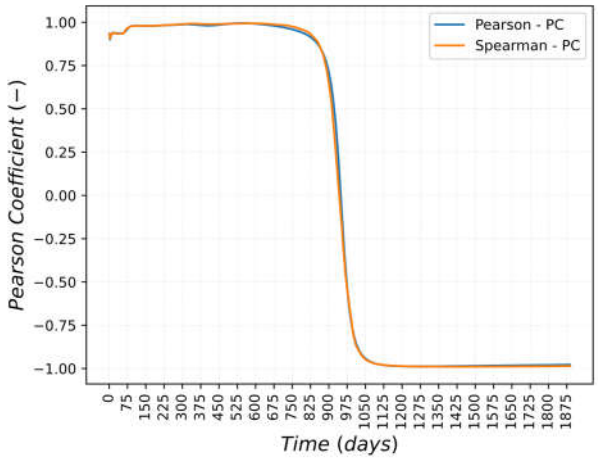

Figure 15. Partial Correlation trend for CuCrZr perturbation

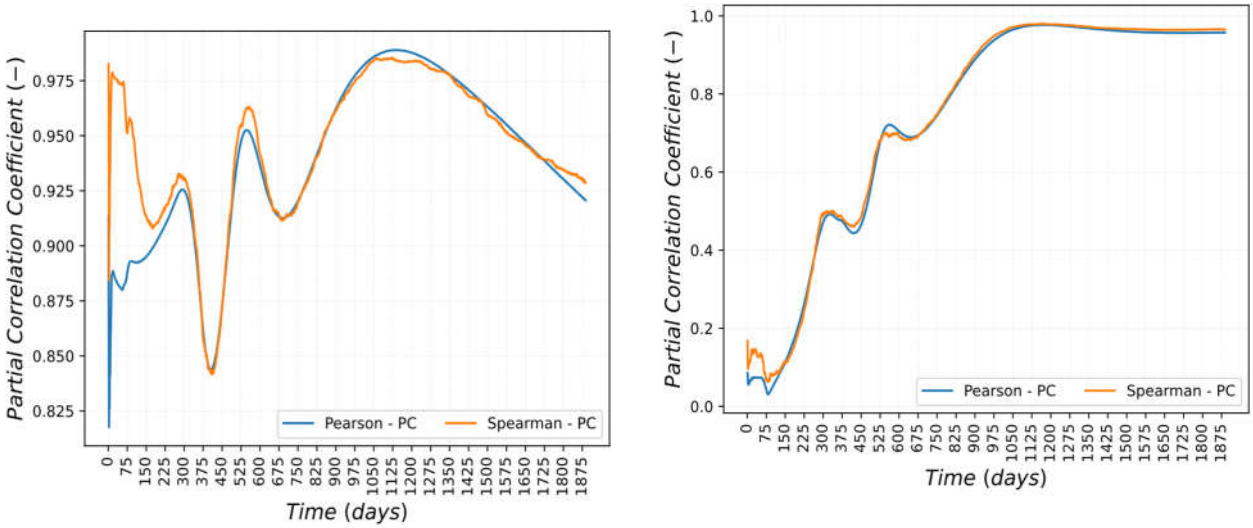

Figure 16. Partial Correlation trend for (a) STCR perturbation; (b) LTCR perturbation

8. Conclusions and future work

The impact of water chemistry on ACPs has been studied through the perturbation of chemical parameters, such as the LiOH concentration and the corrosion rates of different materials. The model used in OSCAR-Fusion V1.3 is a simplified but representative reproduction of the EU-DEMO PFU.

Two different case studies have been analyzed. Case Study 1 demonstrates that, due to the LiOH concentration perturbation, there is an impact on Mn-54 activity in the deposit/outer oxide layer of the whole loop. Case Study 2 shows how the perturbation of normalized corrosion coefficients can significantly impact the Mn-54 activity in the deposit/outer oxide layer.

It has to be noted that the perturbation on LiOH leads to a pH variation in the cooling circuit. The pH is a parameter on which the corrosion rate depends when the Moorea law is set as the corrosion release law. The perturbation of normalized corrosion coefficients

 doi:10.20944/preprints202304.0275.v1

leads to a variation in the cooling circuit's corrosion rate and release rate. The corrosion rate formulation depends on four different parameters: temperature, pH, equilibrium concentration, and normalized corrosion coefficients for the STCR and LTCR.

For Case Study 1, the statistical analysis has shown that the correlation between the perturbed parameter and the Mn-54 activity in the loop's deposit/outer oxide layer is not linear or monotonic. For Case Study 2, the statistical analysis has shown that the correlation between the perturbed parameters and the Mn-54 activity in the deposit/outer oxide layer in the loop is linear and monotonic in most of the scenario considered.

These analyses suggest that the perturbation of the water chemistry composition has an impact on the ACPs but is not always observable with the Pearson and Spearman correlations and Pearson and Spearman partial correlations.

Optimizing the water chemistry leads to a reduction of corrosion products into a coolant loop; this means a reduction of the build-up of ACPs and so the specific activity of one or more components during planned maintenance or at the end of their life cycle. Consequently, with water chemistry control, it is possible to reduce occupational radiation exposure during both the maintenance and the decommissioning phases.

As previously said, OSCAR-Fusion V1.3 does not foresee physical models for radiolysis. As described in [23], there is a more oxidizing environment due to radiolysis with respect to the one modeled by OSCAR-Fusion V1.3; this is due to the presence of free radicals and molecules more oxidizing than O_2, like hydrogen peroxide or hydroperoxide.

Considering the preliminary nature of this water chemistry analysis, more detailed studies will be performed to analyze the impact of oxygen perturbation and other alkalizing agents with a new version of the computer code, OSCAR-Fusion V1.4.

9. Acknowledgments

This work was carried out within the framework of the EUROfusion Consortium, funded by the European Union via the Euratom Research and Training Program (Grant Agreement No 101052200—EUROfusion). Views and opinions expressed are, however, those of the author(s) only and do not necessarily reflect those of the European Union or the European Commission. Neither the European Union nor the European Commission can be held responsible for them.

10. List of Abbreviation

ACP	Activated corrosion products
CB	Cassette body
CFP	Cold feeding pipes
CL	Cold leg
COV	Cross over pipe
CVCS	Chemical volume control system
FOM	Figure of merit
HEX	Heat exchanger
HFP	Hot feeding pipe
HL	Hot leg

 doi:10.20944/preprints202304.0275.v1

IF	In flux
INL	Idaho National Laboratory
IVT	Inner vertical target
LB	Lower bound
LTCR	Long Term Corrosion Rate
MCP	Main coolant pump
OF	Out of flux
OSCAR	Tool for simulating contamination in reactors
OVT	Outer vertical target
PFU	Plasma facing units
PHTS	Primary heat transfer system
PRZ	Pressurizer
PWR	Pressurized water reactor
RP	Reflector plates
SL	Shielding liner
STCR	Short Term Corrosion Rate
UB	Upper bound

References

1. Caruso G. et al., "DEMO – The main achievements of the Pre – Concept phase of the safety and environmental work package and the development of the GSSR", Fusion Engineering and Design, 2022, https://doi.org/10.1016/j.fusengdes.2022.113025
2. Dongiovanni D.N. et al., "DEMO Divertor Cassette and Plasma facing Unit in Vessel Loss-of-Coolant Accident", Energies 2022, 15(23), 8879; https://doi.org/10.3390/en15238879
3. D'Onorio M. et al., "Development of a Thermal-Hydraulic Model for the EU-DEMO Tokamak Building and LOCA Simulation", Energies 2023, 16(3), 1149; https://doi.org/10.3390/en16031149
4. Rafique M. et al., "Review of computer codes for modelling corrosion product transport and activity build-up in light water reactors", Nukleonika, 55 (2010), pp. 263-269
5. Daquait F. et al., "Modelling of the contamination transfer in nuclear reactors: The OSCAR code – applications to SFR and ITER", 1st IAEA Workshop on Challenges for Coolants in Fast Neutron Spectrum Systems, 2017
6. Digby D. M. et al., "A critical review of radiolysis issues in water-cooled fission and fusion reactors: part I, assessment of radiolysis models", Corrosion and Materials Degradation, 2022, pp. 470-535; https://doi.org/10.3390/cmd3030028
7. IAEA, "Reactor water chemistry relevant to coolant-cladding interaction", IAEA-TECDOC-429, 1987
8. Platts L. et al., "Corrosion and chemistry control for the WCLL system with investigation of corrosion mechanisms of Eurofer in aqueous solutions 2020", Report IDM, EDFA_D_2PL25H, 2021
9. Lo Piccolo E. et al., "Preliminary assessment of cooling water chemistry for fusion power plants", Corrosion and Materials Degradation, 2021, 512-530; https://doi:10.3390/cmd2030027
10. D'Onorio M. et al., "RAVEN/OSCAR-Fusion coupling for activated corrosion products assessments, sensitivity and uncertainty quantification", IEEE Transactions on Plasma Science, 2022 (accepted for publication); https://doi:10.1109/TPS.2022.3187784
11. CEA, "La corrosion et l'altération des matèriaux du nuclèaire", CEA Saclay et Group Moniteur (Éditions du Moniteur), Paris, 2010
12. Di Pace L., "Activated corrosion products assessment in fusion reactors", 2019

13. Narcisi V. et al., "WCLL DIV-PFU PHTS DDD (Direct Coupling Option with Small ESS)", Report IDM EDFA_D_2ND5SH, 2020
14. Terranova N., "Activation corrosion products (ACP) assessment", Report IDM, EDFA_D_XYZ123, 2020
15. Terranova N., "ACPs assessment for DEMO Divertor Cooling loop", Report IDM, EDFA_D_2P9QUG, 2022
16. Rabiti C. et al., "RAVEN User Manual", INL/EXT-15-34123,
17. https://inldigitallibrary.inl.gov/sites/sti/sti/Sort_4450.pdf
18. Wilks S. S., "Determination of sample size for setting tolerance limits", The Annals of Mathematical Statistics 12(1), pp. 91-96 (1941)
19. Wilks S. S., "Statistical prediction with special reference to the problem of tolerance limits", The Annals of Mathematical Statistics 13(4), pp. 400-409 (1942)
20. Dodge Y., "Spearman Rank Correlation Coefficient", The Concise Encyclopedia of Statistics, pp. 502-505 (2008); https://doi:10.1007/978-0-387-32833-1_379
21. Kirch W., "Pearson's Correlation Coefficient", The Encyclopedia of Public Health, pp. 1090-1091(2008); https://doi: 10.1007/978-1-4020-5614-7_2569
22. Obitz C. et al., "Erosion corrosion of CuCrZr specimens exposed for simulater ITER operation conditions", Nuclear Materials and Energy, 9 (2016) 261-266; https://doi: 10.1016/j.nme.2016.05.001
23. Harrington C. et al., "Chemistry and corrosion research and development for the water cooling circuits of European DEMO", Fusion Engineering and Design, 146 (2019) 478-481; https://doi.org/10.1016/j.fusengdes.2018.12.095